A Multi-Time-Step Finite Element Algorithm for 3-D Simulation of Coupled Drift-Diffusion Reaction Process in Total Ionizing Dose Effect

Jingjie Xu, Zhaocan Ma, Hongliang Li, Yu Song, Linbo Zhang, and Benzhuo Lu

***Abstract*—In order to study the total ionizing dose degradation and enhanced low dose rate sensitivity effect for semiconductor devices in the space environment, we simulate the drift-diffusion-reaction processes in a 3-dimensional SiO_2–Si system. Since the time scale of the drift-diffusion processes is much larger than that of the chemical reaction processes, we use a multi-time-step algorithm to calculate the two types of processes, respectively. In this paper, partial differential equations used to describe the electrodiffusion processes are solved by a finite element method, while the chemical reactions taking place independently in every mesh node are solved as ordinary differential equations. We reproduce qualitative properties of total ionizing dose effect and compare our numerical results with experimental data and other simulation results. This paper paves a way for 3-D simulation of total ionizing dose and enhanced low dose rate sensitivity with high efficiency and robustness.**

***Index Terms*—Drift-diffusion reaction, ELDRS, finite element method, multi-time-step algorithm, TID.**

I. Introduction

THE DAMAGE induced by total ionizing dose (TID) effect is extremely harmful to semiconductor devices in space. Oxide charge (N_{ot}) and interface traps (N_{it}) are produced during the ionizing radiation period (defined as the ratio of the total dose to the dose rate). Subsequent physical effects, such as the changing of the base current I_B and threshold voltage, will disturb working state of the device. As found in 1991, TID degradation of a bipolar device increases with lower dose rates for a fixed total dose [1]. This phenomenon is referred as enhanced low dose rate sensitivity (ELDRS). Due to ELDRS, bipolar devices should be evaluated under the true dose rate, which implies a rather long time for low dose rate. Numerical simulations of TID and ELDRS provide a way to evaluate the damage at low dose rate shortly and are helpful for exploring the underlying mechanism determining the enhance factor and stress dependence.

In conventional cases, only three unknowns, potential, electron and hole, are considered in semiconductor models, and thus the basic Poisson-Nernst-Planck (PNP) equations, including a Poisson and two Nernst-Planck (NP) equations, are sufficient for describing the drift-diffusion (DD) processes. However, TID and ELDRS processes are more complicated than the conventional cases. We need to simulate radiation induced electron-hole pairs (EHPs), passivation residual H_2 as well as oxygen vacancy defects and their charge states. Besides the increasement of species, chemical reaction processes between these species and the strongly coupled DD process, named as DD reaction processes, lead to a rather complex semiconductor system. In this framework, several different models have been proposed and studied using nonlinear differential equations in view of computational mathematics [2]–[5]. In addition to the above remarkable features, the time step of DD reaction processes is difficult to determine. It is observed that the time scale of DD processes are thousands times larger than that of chemical reactions, and thus it is challenging to solve such a problem with high efficiency.

The DD reaction model has been implemented in numerical simulations in 1D [4] and 2D [5] using finite element and finite volume methods, respectively. Although their numerical results fit with experiments, the simulations are shown to be with low efficiency [4]. For practical devices rather than a simple metal-insulator-semiconductor (MIS) structure, 3D simulations are natural and necessary, which are much more time-consuming compared to 1D and 2D simulations, especially for time-dependent systems. Advanced numerical methods, such as multi-time-step algorithm and restricted additive Schwarz (RAS) preconditioner, have been applied in

Manuscript received September 23, 2017; revised October 31, 2017; accepted November 27, 2017. Date of publication December 1, 2017; date of current version February 1, 2018. This work was supported in part by the Science Challenge Program under Grant TZ2016003-1, in part by the National Key Research and Development Program of Ministry of Science and Technology under Grant 2016YFB0201304, in part by the China NSF under Grant 21573274, Grant 11404300, Grant 91430215, and Grant 91530323, and in part by the National Center for Mathematics and Interdisciplinary Sciences of Chinese Academy of Sciences. *(Corresponding authors: Yu Song; Benzhuo Lu.)*

J. Xu is with the School of Mathematical Sciences, University of Science and Technology of China, Hefei 230026, China, and also with the State Key Laboratory of Scientific and Engineering Computing, Academy of Mathematics and Systems Science, Chinese Academy of Sciences, Beijing 100190, China.

Z. Ma is with the State Key Laboratory of Scientific and Engineering Computing, Academy of Mathematics and Systems Science, Chinese Academy of Sciences, Beijing 100190, China

H. Li and Y. Song are with the Microsystem and Terahertz Research Center, China Academy of Engineering Physics, Chengdu 610000, China, and also with the Institute of Electronic Engineering, China Academy of Engineering Physics, Mianyang 621900, China (e-mail: kwungyusung@gmail.com).

L. Zhang and B. Lu are with the State Key Laboratory of Scientific and Engineering Computing, Academy of Mathematics and Systems Science, Chinese Academy of Sciences, Beijing 100190, China, and also with the School of Mathematical Sciences, University of Chinese Academy of Sciences, Beijing 100049, China (e-mail: bzlu@lsec.cc.ac.cn).

Color versions of one or more of the figures in this paper are available online at http://ieeexplore.ieee.org.

Digital Object Identifier 10.1109/TSM.2017.2779058

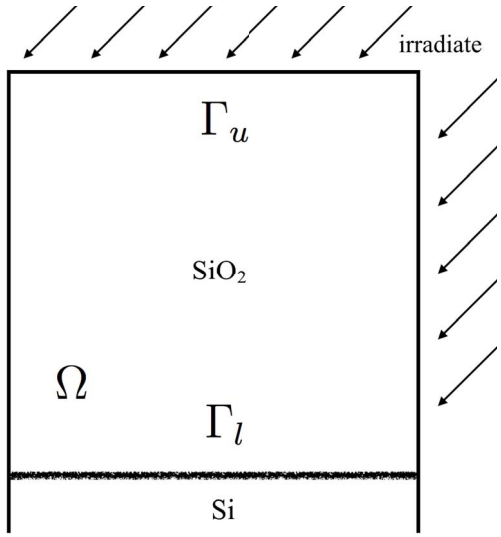

Fig. 1. An illustration showing ionizing dose in a SiO_2-on-Si structure. Ω between the upper boundary Γ_u and the lower boundary Γ_l denotes our computational domain and is simply cuboid.

this work to carry out the numerical simulations with high efficiency and robustness.

In this work, a 3D DD reaction model [5] is simulated with the following special procedures: (1) TetGen Mesh is used to generate high quality tetrahedral meshes suitable for finite element methods. (2) A multi-time-step algorithm is used to deal with different processes. (3) RAS preconditioner [6] is applied to solve the linear systems generated by the finite element method for diffusion-convection equations. The algorithm is implemented based on the parallel finite element toolbox Parallel Hierarchical Grid (PHG) [7]. This is the first work on 3D parallel finite element simulations of ELDRS problem, and the numerical results qualitatively agree with experiments.

This paper is organized as follows. Features of the model are analyzed in Section II. The PDEs and ODEs as well as the multi-time-step algorithm are introduced in Section III. Trends of N_{it} in different situations, the parallel efficiency and parallel scalability are presented in Section IV. And finally the work is summarized in Section V.

II. Model

In our simulations, the SiO_2-on-Si structure is a cuboid and the computational domain of SiO_2 is a cube. Since the geometry is simple, we only present a 2D illustration for the SiO_2-on-Si structure in Figure 1, where the computational domain is the SiO_2 area. The gate is on the upper boundary Γ_u, and the interface traps are generated on the interface Γ_l between the SiO_2 and Si areas. The DD reaction model combines electrodiffusion processes and chemical reaction processes for mobile species, while the non-mobile species only participate in reaction processes. These processes have different time scales, the multi-time-step algorithm used to compute them is discussed in Section III. In this section, we introduce the DD reaction model by discussing trapping species, interface traps, chemical reactions, drift-diffusion reaction equations and boundary conditions. Some details were discussed in Rowsey's work [8].

The trapping species simulated in our work are oxygen vacancies ($V_{o\gamma}$ and $V_{o\delta}$), which are paradigmatic radiation-induced defects in SiO_2 [9]. The neutral oxygen vacancy includes one Si-Si bond instead of two Si-O bonds. Positively charged vacancies have different Si-Si bond situation. From the observation of the defects with electron paramagnetic resonance (EPR) [10], it is found that there are two different kinds of oxygen vacancy centers in amorphous SiO_2, one is a deep hole trap labelled E_γ, and the other is a shallow trap labelled E_δ. The two defects are referred as $V_{o\delta}^+$ and $V_{o\gamma}^+$, while the two neutral precursors are referred as $V_{o\delta}$ and $V_{o\gamma}$ with distinct energies. It is observed from associated energies that $V_{o\delta}^+$ is the shallow one, while $V_{o\gamma}^+$ is much deeper. These two kinds of defects can be hydrogenated or doubly hydrogenated to form $V_{o\gamma}\text{H}$, $V_{o\gamma}\text{H}^+$, $V_{o\gamma}\text{H}_2$, $V_{o\gamma}\text{H}_2^+$, $V_{o\delta}\text{H}$, $V_{o\delta}\text{H}^+$, $V_{o\delta}\text{H}_2$ and $V_{o\delta}\text{H}_2^+$, respectively.

It is known that the accumulation of interface traps changes the electrostatic potential and conductivity inside the semiconductor, and it impairs the function of the insulated gate. The interface traps in metal-oxide-semiconductor (MOS) structures are influenced by radiation-induced electron-hole pairs (EHPs), which are emerged by radiation. In electric field, the holes and electrons are steered and moving towards the interface and metal gate, individually. Then neutral oxygen vacancies become positively charged after capturing holes and then be neutralized by electrons. Protons and hydrogenated defects are created when molecular hydrogen recombines the positively charged defects, and protons can also be cracked by positively-charged hydrogenated defects directly. Finally, interface traps are formed by the reactions of protons and the Si-H bonds on the SiO_2/Si interface. The reaction equation is as follows:

$$\text{H}^+ + \text{Si-H} \Leftrightarrow N_{\text{it}} + \text{H}_2 \tag{1}$$

In this model, 16 different species participate in 20 chemical reactions (See Table I), and thus the reaction process is extremely complicated and difficult to simulate. For convenience, we use recombination and generation terms to stand for chemical reactions in PNP equations, and these terms are nonzero after irradiation. Consider two kinds of the bulk reactions:

$$A + B \Leftrightarrow C \tag{2}$$

and

$$A + L \Leftrightarrow M + N \tag{3}$$

In non-equilibrium conditions, each species has recombination and generation terms. Species A, for example, has the generation term G_A and the recombination term R_A as follows.

$$G_A = k_r^{(A,B),(C)}[C] + k_r^{(A,L),(M,N)}[M][N] \tag{4}$$

$$R_A = k_f^{(A,B),(C)}[A][B] + k_f^{(A,L),(M,N)}[A][L] \tag{5}$$

where k_f and k_r are forward and reverse reaction rates, respectively. A, B, C, L, M and N stand for different species. $[A]$ stands for the concentration of species A. For other species,

TABLE I
REACTION ENERGIES AND RESULTANT k VALUES [8]

chemical reaction	E_f	E_r	k_f	k_r
$V_{o\gamma}+h^+ \Leftrightarrow V_{o\gamma}^+$	0.0	4.5	1.03e-13	1.26e-62
$V_{o\gamma}^+ + H_2 \Leftrightarrow V_{o\gamma}H + H^+$	0.5	0.8	1.92e-19	1.03e-19
$V_{o\gamma}^+ + e^- \Leftrightarrow V_{o\gamma}$	0.4	9.0	1.97e-14	3.21e-138
$V_{o\delta}+h^+ \Leftrightarrow V_{o\delta}^+$	0.0	0.6	1.03e-13	4.16e+3
$V_{o\delta}^+ + H_2 \Leftrightarrow V_{o\delta}H + H^+$	1.4	0.8	1.46e-34	1.03e-19
$V_{o\delta}^+ + e^- \Leftrightarrow V_{o\delta}$	0.0	9.0	2.06e-7	3.21e-138
$V_{o\gamma}H + h^+ \Leftrightarrow V_{o\gamma}H^+$	0.0	4.5	1.03e-13	1.26e-62
$V_{o\gamma} + H^+ \Leftrightarrow V_{o\gamma}H^+$	1.8	2.0	8.21e-37	5.04e-22
$V_{o\gamma}H^+ + e^- \Leftrightarrow V_{o\gamma}H$	0.0	7.5	2.06e-7	5.07e-113
$V_{o\delta}H + h^+ \Leftrightarrow V_{o\delta}H^+$	0.0	0.6	1.03e-13	4.16e+3
$V_{o\delta} + H^+ \Leftrightarrow V_{o\delta}H^+$	0.6	0.4	1.03e-19	3.81e+5
$V_{o\delta}H^+ + e^- \Leftrightarrow V_{o\delta}H$	0.0	3.0	2.06e-7	2.00e-37
$V_{o\gamma}H_2 + h^+ \Leftrightarrow V_{o\gamma}H_2^+$	0.0	0.6	1.03e-13	4.16e+3
$V_{o\gamma}H + H^+ \Leftrightarrow V_{o\gamma}H_2^+$	0.8	0.4	1.03e-19	3.81e+5
$V_{o\gamma}^+ + H_2 \Leftrightarrow V_{o\gamma}H_2^+$	0.6	0.4	4.02e-21	1.90e+5
$V_{o\gamma}H_2^+ + e^- \Leftrightarrow V_{o\gamma}H_2$	0.0	9.0	2.06e-7	3.21e-138
$V_{o\delta}H_2 + h^+ \Leftrightarrow V_{o\delta}H_2^+$	0.0	0.6	1.03e-13	4.16e+3
$V_{o\delta}H + H^+ \Leftrightarrow V_{o\delta}H_2^+$	0.8	0.4	1.03e-19	3.81e+5
$V_{o\delta}^+ + H_2 \Leftrightarrow V_{o\delta}H_2^+$	1.2	0.5	3.35e-31	3.98e+3
$V_{o\delta}H_2^+ + e^- \Leftrightarrow V_{o\delta}H_2$	0.0	9.0	2.06e-7	3.21e-138

the recombination and generation terms are defined in the same way.

The forward and reverse reaction energies E_f and E_r (eV), obtained from first principles calculations employing density functional theory [9], are listed in Table I as well as the reaction rates k_f and k_r. Two different cases are considered: (1) Three species participate in the reaction like Eq. (2). (2) Four species participate in the reaction like Eq. (3). The dimension of k_f is cm^3/s in either case, and dimensions of k_r are different in two cases: 1/s in case (1) and cm^3/s in case (2).

The DD reaction process is mainly described by PNP equations in our model. As all kinds of species participate in chemical reactions, we use generation and recombination terms to simulate the reaction process. Among these species, electrons, holes and H^+ are charged and mobile, their Nernst-Planck equations with G and R terms are shown as follows:

$$\frac{\partial[e^-]}{\partial t} = \nabla \cdot D_{e^-}\left(\nabla[e^-] + e_c\beta[e^-]\vec{E}\right) + U_{\text{radiation}} + G_{e^-} - R_{e^-}, \quad (6)$$

$$\frac{\partial[h^+]}{\partial t} = \nabla \cdot D_{h^+}\left(\nabla[h^+] - e_c\beta[h^+]\vec{E}\right) + U_{\text{radiation}} + G_{h^+} - R_{h^+}, \quad (7)$$

$$\frac{\partial[\mathrm{H}^+]}{\partial t} = \nabla \cdot D_{\mathrm{H}^+}\left(\nabla[\mathrm{H}^+] - e_c\beta[\mathrm{H}^+]\vec{E}\right) + G_{\mathrm{H}^+} - R_{\mathrm{H}^+}. \quad (8)$$

$\vec{E}$ is the electric field, e_c is the elementary charge, D is the diffusion coefficient, e^- denotes the electron, h^+ denotes the hole, $\beta = 1/k_BT$, where k_B is the Boltzmann constant and T is the temperature, and $U_{\text{radiation}}$ is the EHP generation term [11],

$$U_{\text{radiation}} = Y * g_0 * R_d \quad (9)$$

where $Y = 0.01$ is the percent of electrons and holes surviving initial recombination, R_d is the dose rate, the constant g_0 is set to 8.1×10^{12} EHP/rad/cm^3. Hydrogen is mobile, but not charged.

$$\frac{\partial[\mathrm{H}_2]}{\partial t} = \nabla \cdot D_{\mathrm{H}_2}\nabla[\mathrm{H}_2] + G_{\mathrm{H}_2} - R_{\mathrm{H}_2} \quad (10)$$

$V_{o\gamma}$, $V_{o\gamma}^+$, $V_{o\delta}$, $V_{o\delta}^+$, $V_{o\gamma}H$, $V_{o\gamma}H^+$, $V_{o\delta}H$, $V_{o\delta}H^+$, $V_{o\gamma}H_2$, $V_{o\gamma}H_2^+$, $V_{o\delta}H_2$, $V_{o\delta}H_2^+$ are non-mobile defects but taking part in reactions, and therefore the equations of these species become ordinary differential equations (ODEs):

$$\frac{dT_i}{dt} = G_i - R_i \quad (11)$$

which are solved by the forward Euler algorithm in time-dependent simulations.

In a semiconductor, the 9 charged species and applied potential determine the electrostatic field, which is described by the following Poisson equation:

$$-\epsilon\nabla^2\phi = Q_{\mathrm{SiO_2}} \quad (12)$$

$$Q_{\mathrm{SiO_2}} = e_c\left([h^+] + [\mathrm{H}^+] + [V_{o\delta}^+] + [V_{o\delta}\mathrm{H}^+] + [V_{o\delta}\mathrm{H}_2^+] + [V_{o\gamma}^+] + [V_{o\gamma}\mathrm{H}^+] + [V_{o\gamma}\mathrm{H}_2^+] - [e^-]\right) \quad (13)$$

ϕ is the electrostatic potential function ($-\vec{E} = \nabla\phi$), and ϵ is the dielectric coefficient function.

The boundary conditions for the 12 non-mobile species are not needed, because their reaction processes are described by ODEs. On the gate contact and SiO_2/Si interface, the electrons, holes and protons are allowed to move freely, and thus Dirichlet boundary conditions are set for the 3 charged species on these surface. For the H_2 case, the concentration on the gate is constant and equal to the ambient concentration, thus Dirichlet boundary condition is used on the gate. Apart from the mentioned situations, reflection boundary condition is applied on other surfaces for all moving particles. On the Si/SiO_2 interface, H^+ is involved in the key reaction generating interface traps, as shown in Eq. (1). The reverse reaction is assumed to be negligible at room temperature. If we consider the concentration densities of H^+ and SiH on SiO_2/Si interface, the quantitative equation for the density of interface traps is defined as:

$$\frac{dN_{\text{it}}}{dt} = k(\sigma_{\text{SiH}} - N_{\text{it}})J_{\mathrm{H}^+} \cdot \vec{n} \quad (14)$$

where k is the reaction rate for rescaling the rate of the chemical reaction, and $J_{\mathrm{H}^+} = -D_{\mathrm{H}^+}(\nabla[\mathrm{H}^+] - e_c\beta[\mathrm{H}^+]\nabla\phi)$. σ_{SiH} is the initial density of SiH on Γ_l, the density of SiH on Γ_l decreases with the reaction process, and the current density of SiH = $\sigma_{\text{SiH}} - N_{\text{it}}$.

III. METHOD

The tetrahedral mesh of the computational domain (SiO_2) is presented in Figure 2. It is a 1 μm^3 cube subdivided into three subregions, namely upper, middle and lower region, for mesh generation, and the thickness of the three regions are 0.25, 0.5, 0.25 μm, respectively. The mesh density in both upper region and lower region is high, while the mesh density in the middle region is low. The mesh is generated by the widely used software package TetGen [12], and the input parameter

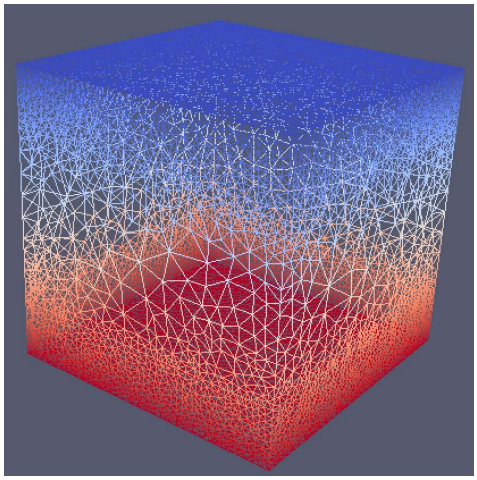

Fig. 2. A mesh including 168986 vertices and 977221 tetrahedra, produced by ParaView [13].

"maximum tetrahedron volume constraint" is used to control the mesh distribution in the subregions. The generated mesh can be directly used in the finite element computations. A good quality mesh is essential to achieve high accuracy and efficiency of the simulations.

Before discussing the multi-time-step algorithm, we introduce the finite element method (FEM) for solving the drift-diffusion-reaction equations [14]. The Nernst-Planck equations are rewritten in a general form.

$$\frac{\partial c_i}{\partial t} = \nabla \cdot D_i(\nabla c_i + \beta q_i c_i \nabla \phi) + F_i, \quad \text{in } \Omega \tag{15}$$

$$-\nabla \cdot \epsilon \nabla \phi = \lambda \sum_i q_i c_i, \quad \text{in } \Omega \tag{16}$$

where i stands for different kind of species, and for the i-th species, c_i is the density distribution function, $q_i = z_i e_c$ is the charge each particle carried. $F_i = U_{\text{radiation}} + G_i - R_i$ for e^- and h^+, while $F_i = G_i - R_i$ for H^+ and H_2, where G_i is the generation term, and R_i is the recombination term. The terms G_i and R_i are nonlinear distribution functions of different species.

For convenience, we nondimensionalize the function of electrostatic potential by introducing a new variable $u = e_c \beta \phi$, then the PNP equations become

$$\frac{\partial c_i}{\partial t} = \nabla \cdot D_i(\nabla c_i + z_i c_i \nabla u) + F_i, \quad \text{in } \Omega \tag{17}$$

$$-\nabla \cdot \epsilon \nabla u = \lambda e_c^2 \beta \sum_i z_i c_i, \quad \text{in } \Omega \tag{18}$$

In this work, the boundary conditions of the electrostatic potential in semiconductor systems are set as

$$u = e_c \beta \phi = 4.1 e_c \beta, \quad \text{in } \Gamma_u \tag{19}$$

$$u = e_c \beta \phi = 0, \quad \text{in } \Gamma_l \tag{20}$$

$$\frac{\partial u}{\partial \vec{n}} = e_c \beta \frac{\partial \phi}{\partial \vec{n}} = 0, \quad \text{otherwise} \tag{21}$$

All faces are set with reflection boundaries for H_2, while for e^-, h^+ and H^+ they are Dirichlet boundaries. The variational

TABLE II
SEMICONDUCTOR WITH DIFFERENT DOPING [17], [18]

Species	Low doping	High doping
H_2	$10^{11} - 10^{20}$ cm^{-3}	$10^{11} - 10^{20}$ cm^{-3}
$V_{o\gamma}$	10^{14} cm^{-3}	10^{15} cm^{-3}
$V_{o\delta}$	10^{18} cm^{-3}	10^{18} cm^{-3}
$V_{o\gamma}H$	10^{14} cm^{-3}	10^{14} cm^{-3}
$V_{o\delta}H$	10^{14} cm^{-3}	10^{14} cm^{-3}
$V_{o\gamma}H_2$	10^{14} cm^{-3}	10^{16} cm^{-3}
$V_{o\delta}H_2$	10^{13} cm^{-3}	10^{16} cm^{-3}
Si-H	10^{13} cm^{-2}	10^{13} cm^{-2}

form of the dimensionless PNP equations are as follows,

$$\int_\Omega \frac{\partial c_i}{\partial t} \psi dV = -\int_\Omega D_i(\nabla c_i \cdot \nabla \psi + z_i c_i \nabla u \cdot \nabla \psi) dV + \int_\Omega F_i \psi dV, \tag{22}$$

$$\int_\Omega \epsilon \nabla u \cdot \nabla \psi dV = \lambda e_c^2 \beta \sum_i z_i \int_\Omega c_i \psi dV, \tag{23}$$

where ψ is a test function.

For the 16 species, the initial concentrations are uniformly distributed, and only 4 species are mobile. Nonzero initial bulk concentration of the species are shown in Table II. For different kinds of semiconductor, the doping situation changes, but the simulations remain time-consuming and dependent on mesh. The linear system for the high doping case is much more difficult to solve and the RAS preconditioner is required, which is the cheaper and faster variant of the classical additive Schwarz preconditioner (AS) [15], [16]. Since the computation time is very long even using parallel computing, we have only computed with the total dose of 0.1 krad, which is less than in the experiment. The actual simulation time for each data point in the H_2 trend is about 3000 seconds, which is much faster than the simulation time in Rowsey's work [4].

If we only use the finite element method mentioned above, it would take a long time (about 10^9 seconds) to finish the simulation [4], since a very small time step is necessary for the time scale of chemical reaction processes. The time scale of generation and recombination terms are much smaller than that of convection and diffusion terms. For example, if we consider the $V_{o\gamma}H_2^+$:

$$\begin{aligned}\frac{\partial [V_{o\gamma}H_2^+]}{\partial t} &= 1.03\text{e-}13\left[V_{o\gamma}H_2\right]\left[h^+\right] + 1.03\text{e-}19\left[V_{o\gamma}\right]\left[H^+\right] \\ &\quad + 4.02\text{e-}21\left[V_{o\gamma}^+\right][H_2] + 3.21\text{e-}138\left[V_{o\gamma}H_2\right] \\ &\quad - 5.75\text{e+}5\left[V_{o\gamma}H_2^+\right] - 2.06\text{e-}7\left[V_{o\gamma}H_2^+\right]\left[e^-\right]\end{aligned}$$

By rough estimate, the above equation is simplified as follows,

$$\frac{\partial \left[V_{o\gamma}H_2^+\right]}{\partial t} = -C_1(t)\left[V_{o\gamma}H_2^+\right] + C_2(t), \tag{24}$$

where $C_1(t) = 5.75\text{e+}5+2.06\text{e-}7[e^-] > 5.75\text{e+}5$, $C_2(t) \in C^2[0, T]$ and is bounded from above. To discretize the equation, the time step should be much less than 10^{-5} second, and it will take too much time to solve mobile species by FEM using the same time step.

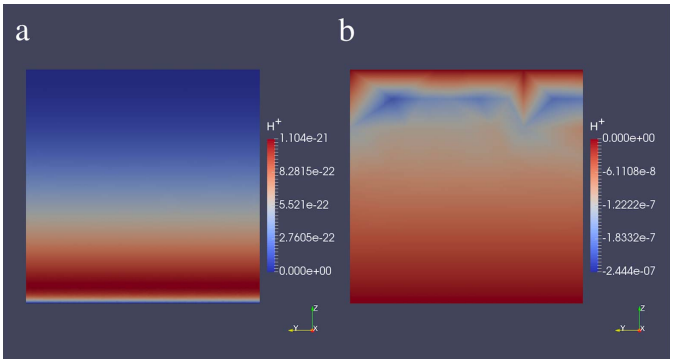

Fig. 3. Distribution of H^+ (a) with and (b) without multi-time-step methods.

In order to accelerate the simulation, a multi-time-step algorithm is introduced. As the differences between the reaction time scales of every two species are much smaller compared with the differences between the time scales of DD and reaction processes, we only use two time steps to simulate the system, namely a macro time step h for DD processes and a micro time step τ for reaction processes. It is assumed that $h = K\tau$, where K is set to 1000 in our semiconductor model. The multi-time-step algorithm is described below, where $f_i = U_{\text{radiation}}$ for e^- and h^+ and $f_i = 0$ for H^+ and H_2. Eq. (25) and (26) indicate the central algorithms in this work. In addition, a preconditioned GMRES method is applied to solve the linear system in the finite element method for efficiency.

S1. Set $n = 0$, $t = 0$, initialize the bulk concentration for every species $[c_1^0, \ldots, c_{16}^0]$ with data in Table II (the species not listed in Table are initialized with 0 mM) and calculate potential u^0 using Poisson Equation.

S2. Set $n = n + 1$, $t = nh$. If $t \leq T$, then set $m = 0$, $[u^{n,0}, c_1^{n,0}, \ldots, c_{16}^{n,0}] = [u^{n-1}, c_1^{n-1}, \ldots, c_{16}^{n-1}]$; otherwise stop the algorithm.

S3. Set $m = m + 1$, solve $c_i^{n,m}$ in Eq. (25) for 4 mobile species using FEM.

$$\int_\Omega \left[c_i^{n,m}\psi + hD_i\left(\nabla c_i^{n,m} + z_i c_i^{n,m}\nabla u^{n,m-1}\right)\cdot\nabla\psi \right] dV = \int_\Omega \left(c_i^{n-1} + hf_i\right)\psi\, dV, \tag{25}$$

S4. Set $k = 0$, $[c_1^{n,m,0}, \ldots, c_{16}^{n,m,0}] = [c_1^{n,m}, \ldots, c_{16}^{n,m}]$

S5. Set $k = k + 1$. If $k > K$, then go to S6; otherwise solve $c_i^{n,m,k}$ in Eq. (26) for every species and repeat S5.

$$c_i^{n,m,k} - c_i^{n,m,k-1} = \tau\left(G_i^{n,m,k-1} - R_i^{n,m,k-1}\right). \tag{26}$$

S6. Solve $u^{n,m}$ in Eq. (27)

$$\int_\Omega \epsilon\nabla u^{n,m}\cdot\nabla\psi = \lambda e_c^2\beta\sum_i z_i\int_\Omega c_i^{n,m,K}\psi, \tag{27}$$

S7. If $||u^{n,m} - u^{n,m-1}|| < \text{tol}$, set $[u^n, c_1^n, \ldots, c_{16}^n] = [u^{n,m}, c_1^{n,m}, \ldots, c_{16}^{n,m}]$ and go to S2; otherwise go to S3.

To justify the necessity of the multi-time-step algorithm, we compare the numerical results with and without the muti-time-step algorithm, as shown in Figure 3. Reasonable concentration results are obtained by using the multi-time-step algorithm with a macro time step h and a micro time step τ (Figure 3(a)), and wrong results with negative concentration are obtained if the same time step h is used for both the DD and the reaction processes (Figure 3(b)).

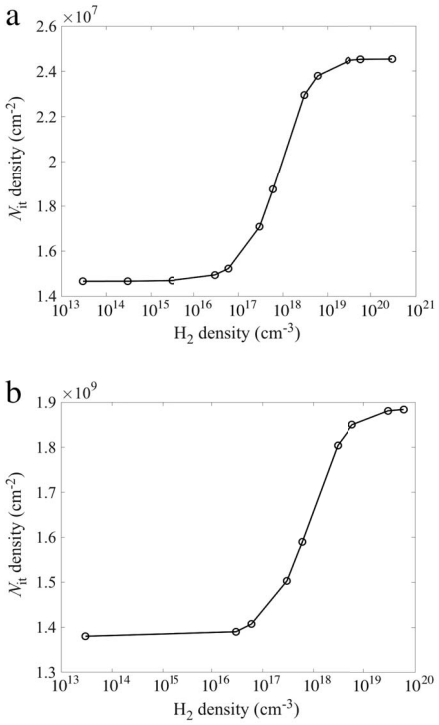

Fig. 4. N_{it} concentration as a function of H_2 density with total dose of 0.1 krad at 10 rad/s in (a) low doping and (b) high doping.

Furthermore, the algorithm will be optimized as follows: each species in the simulation has a special pair of macro time step and micro time step according to its diffusion rate and sensitivity to chemical reaction. For example, since H^+ and H_2 have low diffusion rates and are not sensitive to chemical reactions, the time scales of the DD and the reaction processes for the two species are large (h and τ should be large). It is believed that if more time steps are used for different species, the simulation will be even faster, which will be studied in our further work. In this work, we only use two time steps to accelerate the simulation.

IV. Numerical Results

We have implemented a parallel program for the algorithm described in the last section. The program is based on the parallel FEM toolbox PHG [7], which is coded in C and uses mesh partitioning and MPI for parallel computing. The numerical simulations presented here were carried out on the cluster LSSC-III of the State Key Laboratory of Scientific and Engineering Computing of Chinese Academy of Sciences, which consists of compute nodes with dual Intel Xeon X5550 quad-core CPUs, interconnected via DDR InfiniBand network.

Figure 4 shows the trend of N_{it} data in different H_2 concentrations, which matches the data trend observed in the experiments [2]. The high doping case has a swift change despite the similar trend, which could be explained by the

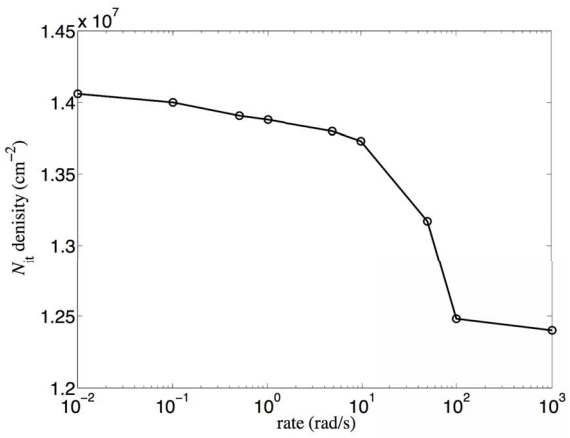

Fig. 5. N_{it} concentration as a function of dose rate with total dose of 0.1 krad and the H_2 density of 3×10^{14} cm^{-3}.

higher chance of the direct release of double-hydrogenated defects. Protons can be generated by coupling H_2 cracking mechanism and direct proton release mechanism. It has been reported that the cracking mechanism takes the dominant place at medium and high concentrations of H_2, while the direct release mechanism is dominant at low H_2 concentrations [5]. However, the low doping case has a bigger gap (more than 60% up), and it could be explained by the different proportion of defect concentration, like $V_{o\gamma}$, which plays an important role in TID and ELDRS simulations [8]. The initial concentrations difference may explain the difference in the two subfigures. In experiments, the total dose is about 10 krad, and if the dose rate is set to 10 rad/s, the simulation time is 1000 s, which costs too much time in numerical calculation with micro step $\tau < 10^{-5}$ s and macro step $h < 10^{-1}$ s. Therefore, we only simulated the system with the total dose of 0.1 krad.

Figure 5 shows the influence of dose rate on N_{it} concentration, which matches the trend of experiment data and the simulation result of 1D case [3], [19]. The quantities of interface traps decrease with the increase of dose rate at a given total dose.

It is found that the image of numerical results shifts rightward comparing with the experiment, and this phenomena also occurs to the H_2 trend. In fact, the parameter Y in Eq. (9), chosen between 0.0 and 1.0, greatly influenced the profiles of H_2 trend. The larger the Y is, the trend shifts more leftward. Y is set to 0.01 according to previous work about MOS devices [20]. Besides, the numerical results are influenced by other parameters [19] and the density distributions of defects in SiO_2 [18], [21].

It is worth noting that though the simulations reproduce similar trends as in experiments' results and others' computational predictions, however, it is found that the numerical results of interface trap concentrations are influenced by lots of facts, such as the size of the semiconductor, the mathematical model, boundary conditions, different doping cases, different concentrations of the defects and various parameters. Due to those reasons, the order of numerical results may not coincide well with experiment data. In next step, we will try to explore the TID and ELDRS effect under various conditions and study the mechanisms behind them in order to present better characterizations in our future work.

TABLE III
PARALLEL EXTENDABILITY

Num of procs	Times	Efficiency
32	182000 s	100%
64	75888 s	120%
128	30444 s	149%
256	16566 s	137%
512	14570 s	78%
1024	16990 s	33%

In order to assess the parallel scalability of our program with 1024 processes, we simulate a much larger system with a mesh containing 1418778 vertices and 8637254 tetrahedra. Table III gives the wall-clock time and parallel efficiency for different number of MPI processes. Because the memory requirement is large, our tests start with 32 processes, whose parallel efficiency is regarded as 100%, and the parallel efficiency for p processes is defined as:

$$E_p = \frac{32T_{32}}{pT_p} \tag{28}$$

where T_p denotes the time to solve the PNP equations using p processes for irradiating 0.1 krad with the rate of 10 rad/s. In most cases, our program has good parallel scalability.

There is a sharp drop in the parallel efficiency from 512 processes to 1024 processes, which has also been observed on the cluster LSSC-III with some other programs. The cause of this phenomenon is considered to be related to the interconnection topology of the underlying InfiniBand network.

V. CONCLUSION

We design an algorithm consisting of a FEM and a multi-time-step algorithm for numerical simulations of the time-dependent drift-diffusion-reaction processes for ELDRS in semiconductor devices. This algorithm can give a better description of the proton concentration than previous simulations. A parallel program for this algorithm is implemented based on the parallel finite element toolbox PHG. 3D numerical simulations are carried out for the first time, and the numerical results qualitatively match with experiments.

REFERENCES

[1] E. W. Enlow, R. L. Pease, W. Combs, R. D. Schrimpf, and R. N. Nowlin, "Response of advanced bipolar processes to ionizing radiation," *IEEE Trans. Nucl. Sci.*, vol. 38, no. 6, pp. 1342–1351, Dec. 1991, doi: 10.1109/23.124115.

[2] X. J. Chen *et al.*, "Mechanisms of enhanced radiation-induced degradation due to excess molecular hydrogen in bipolar oxides," *IEEE Trans. Nucl. Sci.*, vol. 54, no. 6, pp. 1913–1919, Dec. 2007, doi: 10.1109/TNS.2007.909708.

[3] R. L. Pease *et al.*, "The effects of hydrogen on the enhanced low dose rate sensitivity (ELDRS) of bipolar linear circuits," *IEEE Trans. Nucl. Sci.*, vol. 55, no. 6, pp. 3169–3173, Dec. 2008, doi: 10.1109/TNS.2008.2006478.

[4] H. P. Hjalmarson, R. L. Pease, and R. A. B. Devine, "Calculations of radiation dose-rate sensitivity of bipolar transistors," *IEEE Trans. Nucl. Sci.*, vol. 55, no. 6, pp. 3009–3015, Dec. 2008, doi: 10.1109/TNS.2008.2007487.

[5] N. L. Rowsey *et al.*, "A quantitative model for ELDRS and H_2 degradation effects in irradiated oxides based on first principles calculations," *IEEE Trans. Nucl. Sci.*, vol. 58, no. 6, pp. 2937–2944, Dec. 2011, doi: 10.1109/TNS.2011.2169458.

[6] X.-C. Cai and M. Sarkis, "A restricted additive schwarz preconditioner for general sparse linear systems," *SIAM J. Sci. Comput.*, vol. 21, no. 2, pp. 792–797, 1999, doi: 10.1137/S106482759732678X.

[7] L. B. Zhang, "A parallel algorithm for adaptive local refinement of tetrahedral meshes using bisection," *Numer. Math. Theory Methods Appl.*, vol. 2, no. 1, pp. 65–89, 2009.

[8] N. L. Rowsey, "Quantitative modeling of total ionizing dose reliability effects in device silicon dioxide layers," Ph.D. dissertation, Dept. Elect. Comput. Eng., Univ. Florida, Gainesville, FL, USA, 2012.

[9] P. E. Blöchl, "First-principles calculations of defects in oxygen-deficient silica exposed to hydrogen," *Phys. Rev. B, Condens. Matter*, vol. 62, no. 10, pp. 6158–6179, 2000, doi: 10.1103/PhysRevB.62.6158.

[10] S. T. Pantelides *et al.*, "The E' center and oxygen vacancies in SiO_2," *J. Non Cryst. Solids*, vol. 354, no. 2, pp. 217–223, 2008, doi: 10.1016/j.jnoncrysol.2007.08.080.

[11] T. R. Oldham, *Ionizing Radiation Effects in MOS Oxides*. Singapore, World Sci., 2000.

[12] H. Si, "TetGen, a delaunay-based quality tetrahedral mesh generator," *ACM Trans. Math. Softw.*, vol. 41, no. 2, pp. 1–36, 2015, doi: 10.1145/2629697.

[13] J. Ahrens, B. Geveci, C. Law, "ParaView: An end-user tool for large data visualization," in *Visualization Handbook*. Amsterdam, The Netherlands: Elsevier, 2005, pp. 717–731, doi: 10.1016/B978-012387582-2/50038-1.

[14] B. Tu *et al.*, "A parallel finite element simulator for ion transport through three-dimensional ion channel systems," *J. Comput. Chem.*, vol. 34, no. 24, pp. 2065–2078, 2013, doi: 10.1002/jcc.23329.

[15] N. Seoane and A. J. García-Loureiro, "Study of parallel numerical methods for semiconductor device simulation," *Int. J. Numer. Model. Electron. Netw. Devices Fields*, vol. 19, no. 1, pp. 15–32, 2006, doi: 10.1002/jnm.596.

[16] T. F. Chan and T. P. Mathew, "Domain decomposition algorithms," *Acta Numerica*, vol. 3, no. 3, pp. 61–143, 1994, doi: 10.1017/S0962492900002427.

[17] W. L. Warren *et al.*, "Links between oxide, interface, and border traps in high-temperature annealed Si/SiO_2 systems," *Appl. Phys. Lett.*, vol. 64, no. 25, pp. 3452–3454, 1994, doi: 10.1063/1.111943.

[18] R. A. B. Devine, D. Mathiot, W. L. Warren, D. M. Fleetwood, and B. Aspar, "Point defect generation during high temperature annealing of the $Si-SiO_2$ interface," *Appl. Phys. Lett.*, vol. 63, no. 21, pp. 2926–2928, 1993, doi: 10.1063/1.110275.

[19] X. J. Chen *et al.*, "Modeling the dose rate response and the effects of hydrogen in bipolar technologies," *IEEE Trans. Nucl. Sci.*, vol. 56, no. 6, pp. 3196–3202, Dec. 2010, doi: 10.1109/TNS.2009.2034154.

[20] M. R. Shaneyfelt, D. M. Fleetwood, J. R. Schwank, and K. L. Hughes, "Comparison of low-energy x-ray and cobalt-60 irradiations of MOS devices as a function of gate bias," presented at the IEEE Int. Nucl. Space Radiat. Effects Conf., 1991, p. 5.

[21] T. W. Sigmon, W. K. Chu, E. Lugujjo, and J. W. Mayer, "Stoichiometry of thin silicon oxide layers on silicon," *Appl. Phys. Lett.*, vol. 24, no. 3, pp. 105–107, 1974, doi: 10.1063/1.1655112.

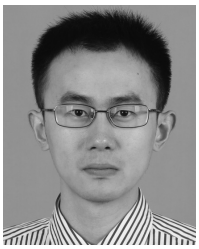

Jingjie Xu was born in 1990. He received the B.S. degree from the University of Science and Technology of China, Hefei, China, in 2013, where he is currently pursuing the Ph.D. degree in computational mathematics with the School of Mathematical Sciences.

Zhaocan Ma received the B.S. degree in mathematics and applied mathematics from Beihang University, Beijng, China, in 2015. He is currently pursuing the Ph.D. degree with the Institute of Computational Mathematics and Scientific/Engineering Computing, Chinese Academy of Sciences, Beijing.

Hongliang Li received the B.S. degree in mathematics from Sichuan University, Chengdu, China, in 2010 and the Ph.D. degree in computational mathematics from the Academy of Mathematics and Systems Science, Beijing, China, in 2015.

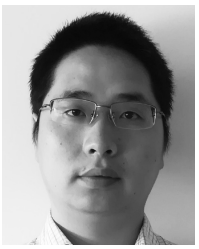

Yu Song received the B.S. degree in physics from Lanzhou University, Lanzhou, China, in 2008 and the Doctoral degree in physics from Tsinghua University, Beijing, China, in 2013. He is currently with the China Academy of Engineering Physics, Chengdu, China, focusing on radiation effects and 2-D materials.

Linbo Zhang was born in 1962. He received the Ph.D. degree in mathematics from Université de Paris-sud, France, in 1987. He is currently a Professor with the Academy of Mathematics and Systems Science, Chinese Academy of Sciences. His research interests include numerical algorithms and high performance computing.

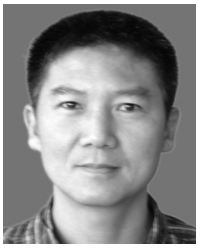

Benzhuo Lu was born in 1970. He received the Ph.D. degree in biochemistry and molecular biology from the University of Science and Technology of China in 2002. He is currently a Professor with the Academy of Mathematics and Systems Science, Chinese Academy of Sciences. His research interests include computational biology/chemistry, numerical methods, and application software.